ACS OMEGA

Open Access

http://pubs.acs.org/journal/acsodf

Article

Study on the Adsorption Law of *n*-Pentane in Silica Slit Nanopores

Cao Yu,* Qinglong Xu, Fancong Meng, Xuwei Liang, Yahui Li, Xin Kang, Hao Lu, Qiubo Wu, and Sen Yang

Cite This: *ACS Omega* 2024, 9, 40145−40153

Read Online

ACCESS | Metrics & More | Article Recommendations

ABSTRACT: As the main components of shale, inorganic minerals are important carriers for oil and gas adsorption, whose pore structures and surface properties have significant effects on the fluid adsorption capacity. In this study, slit nanopores (SNPs) were constructed by silica. To investigate the microscopic adsorption law of *n*-pentane in silica, the grand canonical Monte Carlo (GCMC) method was used to simulate the adsorption behaviors of *n*-pentane in silica nanoparticles. The effects of different surface wettability, pore size, temperature, and pressure values on the adsorption behavior of pentane were discussed, revealing the micro adsorption mechanism of pentane in silica with different pore sizes and wettability and evaluating the degree of oil and gas utilization. The research results indicate that the adsorption capacity of pentane is greatly affected by the temperature under low-pressure conditions. With the increase of the pore size, the adsorption capacity of pentane increases linearly, and the number of adsorbed pentane molecules gradually decreases. The availability of oil and gas increases, and the oil and gas are more easily extracted. As the surface hydrophobicity of minerals increases, the van der Waals force between minerals and pentane also increases, leading to an increase in the number of adsorbed states of pentane. The stronger the hydrophilicity of the wall, the fewer the pentane molecules adsorbed on the surface, which would improve the efficiency of oil and gas extraction. This study provides potential for the development of novel surfactants based on adsorption selectivity.

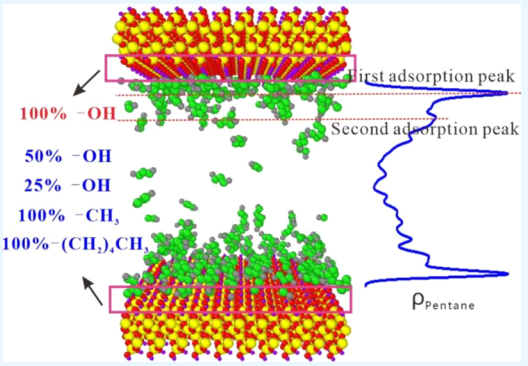

1. INTRODUCTION

With the growth of global energy demand and the continuous decline of conventional oil and gas production, the exploration and development of unconventional oil and gas with great potential have become an attractive research field. Shale gas is an unconventional gas that is reserved in organic-rich shale. The occurrence states of shale gas in reservoirs mainly include free, adsorbed, and dissolved states.[1] According to statistics, adsorbed gas accounts for 20−85% of the total shale gas reserves, and the surface of the nanopore provides a huge adsorption space for them.[2,3] Therefore, researching the fluids' adsorption on mineral surfaces is of great significance for understanding the occurrence states and quantitatively evaluating the adsorption capacity of natural gas underground.

Recently, a large number of experimental studies have been conducted on the adsorption behavior of alkane molecules in nanoparticles.[4−10] Isothermal adsorption experiments were carried out on shale samples to analyze the effects of temperature, pressure, and aperture on alkane adsorption capacity. Liu et al.[11] used graphite slits instead of shale pores to study the adsorption phenomenon of methane gas in shale pores and analyzed the density distribution of methane at different slit sizes and temperatures. However, it did not explain the effect of temperature on adsorption, and the adsorption amount was not quantitatively expressed but characterized by densities. On the basis of temperature variations, Chen et al.[12] further researched the influence of pressure and pore surface water on methane adsorption, and it was found that the presence of water on the slit surface could weaken the adsorption effect. However, their work did not represent the adsorption amount quantitatively either. Tian et al.[13] established a complex molecular model of kerogen based on its elemental content and molecular structure and discussed the effects of temperature, pressure, kerogen molecular composition, and specific surface area on methane adsorption. Amirmoshiri et al.[14] researched the effect of anionic surfactants on the dynamic adsorption of C_{14}−C_{16} at high temperatures of reservoir conditions. The results showed that laboratory surfactant adsorption tests need to take the surfactant wettability and redox state into account. Zhu et al.[15] used the density functional theory (DFT) method with D3 dispersion correction to research the surface adsorption mechanism of methane. They revealed that the interactions

Received: July 1, 2024
Revised: August 19, 2024
Accepted: August 27, 2024
Published: September 11, 2024

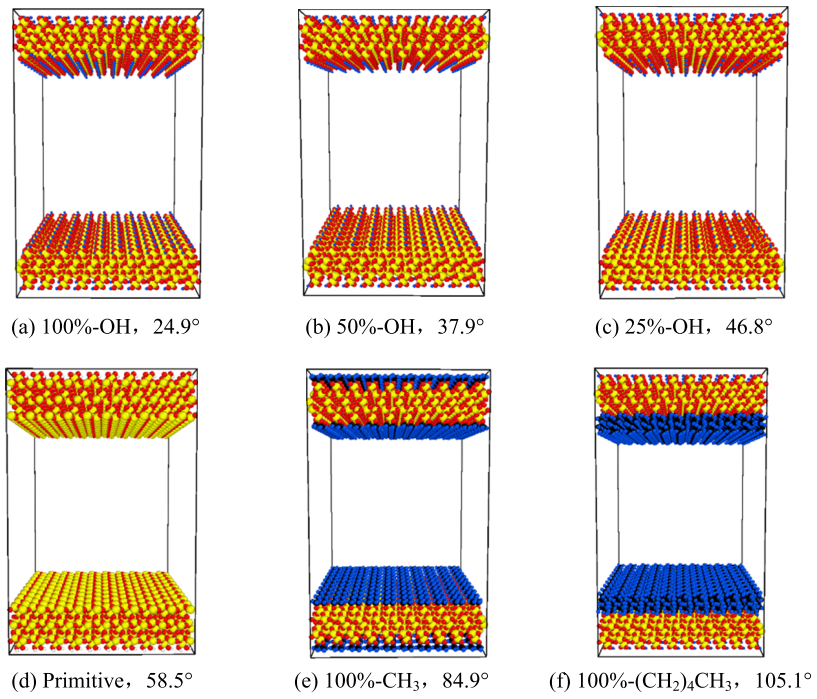

Figure 1. Initial configuration of each group-modified slit at 5 nm (red solid circle: oxygen atom, yellow solid circle: silicon atom, blue solid circle: hydrogen atom, and black solid circle: carbon atom).

between methane and kerogen were van der Waals interactions, which indicated that fluid adsorption on kerogen was physical adsorption. Experimental studies have shown that aperture, pressure, temperature, and mineral surface wettability can obviously affect the adsorption behavior of hydrocarbon fluids in nanopores. However, these studies aim to evaluate the minerals' adsorption capacity to hydrocarbon fluids, which are considered macroscopic adsorption behaviors and cannot be used to analyze the interaction forces between fluids and interfaces in micro-nanopores. Therefore, in this work, molecular simulations were used to study the adsorption behaviors and micromechanism of alkanes in micro-nanopores.

As a theoretical research method, molecular simulations have been widely used in studying adsorption performance.[16−20] Collell et al.[21] conducted molecular simulations on the adsorption of methane/ethane mixtures in artificially formed spherical pores within mature kerogen. At pressures ranging from 1 to 20 MPa, they observed the confinement effect of micropore size, leading to deviations of molecular simulation results from classical adsorption models (i.e., extended Langmuir model and ideal adsorbed solution model). Zhou et al.[22] used the GCMC method to investigate the adsorption behaviors of methane, ethane, and propane mixtures in the kerogen slit pores. Onawole et al.[23] studied the adsorption behaviors of methane on the surface of silica−kaolinite using DFT and molecular dynamics (MD) methods, revealing that methane adsorption is physical adsorption. Jang et al.[24] simulated the adsorption of methane and carbon dioxide in Illite slits using the GCMC method and indicated that van der Waals forces generally existed between gas and solid molecules. For larger adsorbed molecules, the influence of the confinement on the thermodynamic and dynamic properties of the adsorbed phase is even stronger.[25] Chen et al.[26] used the GCMC method to investigate the adsorption behaviors of methane, nitrogen, and carbon dioxide on organic/inorganic minerals at 333 K and found that the interaction between gas molecules also had an effect on the adsorption behavior. Based on the molecular simulation method, previous studies on shale minerals have mainly focused on kerogen,[27−29] montmorillonite,[7,30] Illite,[31] kaolinite,[32] calcite,[33] etc. Quartz, as the main component of shale minerals,[34] has high research value. Besides, small-molecule gases such as methane and ethane[35−40] have been extensively studied, whereas larger molecules have received comparably less attention. Pentane, as one of the main heavy hydrocarbons of shale gas, also has significant research value. The adsorption capacity of minerals is affected by numerous factors. Wettability, standing out as a crucial surface property of solids, cannot be overlooked in its influence on the minerals' capacity to adsorb fluids. In this study, the GCMC method was used to investigate the adsorption behaviors of *n*-pentane in silica nanoparticles with various temperatures and pressures. Based on the simulation results, the micro adsorption mechanism of pentane in silica was analyzed, and a quantitative relationship among nanopore sizes, wettability, and the pentane adsorption amount was established. The simulation results indicate a significant relationship between oil and gas adsorption and mineral surface wettability and pore size. By the simulation results, it is possible to predict the changes in the underground fluid composition during oil and gas extraction, providing guidance for the development of shale oil and gas technology in the future.

2. METHODOLOGY

2.1. Modeling. In this paper, the adsorption law and phase change of *n*-pentane in slits with different pore sizes (2, 3, 5, 7, 9, and 11 nm) and silica nanoslits modified with different functional groups (100%-OH, 50%-OH, 25%-OH, 100%-CH_3, 100%-$(CH_2)_4CH_3$) and unmodified were studied. We first took the 5 nm slit as an example. We selected α-quartz single cell as the base model unit structure. The lattice parameters were as follows: $a = b = 4.913$ Å, $c = 5.4052$ Å, $\alpha = \beta = 90°$,

https://doi.org/10.1021/acsomega.4c06105
ACS Omega 2024, 9, 40145−40153

and $\gamma = 120°$. The (1 0 0) surface was cleaved, and a 10 × 10 supercell was used as the quartz mineral floor to build the slit model. The slit spacing was adjusted to 5 nm, and finally, the slit model was modified by each group, as shown in Figure 1. The wetting contact angle of the slit model modified by each group is referred to in ref 41. We can change the aperture size by translating the upper surface of the slit up or down while also adjusting the simulation system to the corresponding size. Methyl is obtained by adding carbon atoms to the exposed oxygen atoms of silica and then the saturated hydrogenation of carbon atoms. The pentyl group is obtained by adding a carbon chain of five atoms to the oxygen atom and then by saturated hydrogenation of the carbon chain.

2.2. Potential Models. In this paper, the NERD[42] molecular model of *n*-pentane defines the non-bonding interactions of *n*-pentane as non-bonding interactions between different atoms of different molecules and between atoms with a distance greater than three covalent bonds in the same molecule. The Lennard-Jones parameters and charge parameters are listed in Table 1.

Table 1. Non-Bonding Interaction Parameters

atomic type	M (g/mol)	Q (e)	σ (nm)	ε (kJ/mol)
CH_3	15.035	0	0.391	0.2023
CH_2	14.027	0	0.393	0.0914

The corresponding parameters can be determined by the Lorentz−Berthelot mixing rule, as shown in the following formula,[43] and the L-J potential energy parameters of silica substrate atoms are shown in Table 2.

$$\varepsilon_{ij} = \sqrt{\varepsilon_i \varepsilon_j},\ \sigma_{ij} = (\sigma_i + \sigma_j)/2 \quad (1)$$

Table 2. L-J Potential Energy Parameters of Silica Substrate Atoms

atomic type	σ (Å)	ε (kcal/mol)
O	2.708	0.3676
Si	3.905	0.04
H (in −OH)	0	0
O (in −OH)	3.07	0.17
$-CH_3$	3.905	0.175

Non-bonding interactions refer to non-covalent bonding interactions between different molecules or atoms within a molecule, including Coulomb interactions and van der Waals interactions. Van der Waals interactions describe the repulsive or attractive interactions between atoms caused by non-covalent bonds and non-electrostatic forces. The intermolecular interaction between SiO_2 nanoslits and *n*-pentane is represented by the Lennard-Jones 12-6 potential as follows

$$V_{LJ}r_{ij} = 4\varepsilon_{ij}\left[\left(\frac{\sigma_{ij}}{r_{ij}}\right)^{12} - \left(\frac{\sigma_{ij}}{r_{ij}}\right)^{6}\right] \quad (2)$$

where $V_{LJ}(r_{ij})$ is the van der Waals interaction between atom i and atom j, r_{ij} is the distance between two virtual atoms in molecule i and molecule j, σ_{ij} is the scale parameter of the L-J potential energy between two virtual atoms in i and j molecules, and ε_{ij} is the energy parameter of L-J potential energy between two virtual atoms in i and j molecules.

2.3. Simulation Details. In this paper, the Monte Carlo simulation method is used to study the phase change of *n*-pentane in different wettabilities and pore size slits (confined phase). Periodic boundary conditions (PPP) are used in the X, Y, and Z directions. The truncation radius of the L-J force between the particles is 1.2 nm. Nanoslits were fixed in the simulation to reduce computational complexity without affecting the calculation results. The total number of simulation steps is 2 million to obtain the results after full simulation equilibrium. The time step of the GCMC simulation is Δt = 1 fs. The position coordinate information on the particles is output every 2000 steps, and the simulation data are calculated by LAMMPS software.

3. RESULTS AND DISCUSSION

3.1. Changes in Pentane Adsorption with Temperature and Pressure. The pentane adsorption isotherm in the hydroxy-modified silica slit was calculated, as shown in Figure 2. The calculation formula is shown in eq 3. It can be seen that

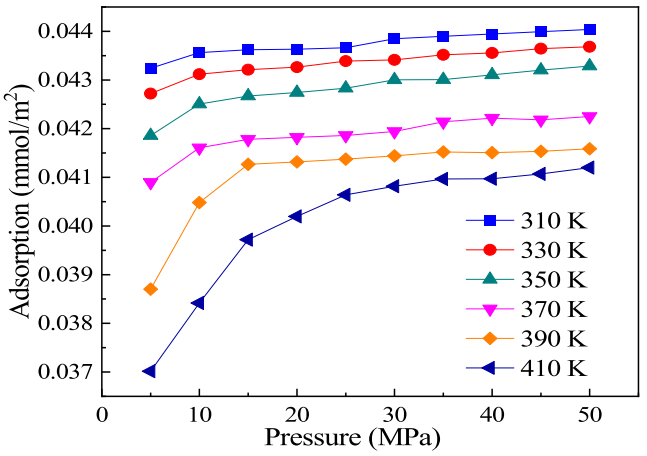

Figure 2. Hydroxyl-modified 5 nm isothermal adsorption line.

the adsorption amount of pentane increases with the increase of pressure. When the pressure is less than 10 MPa, the adsorption of pentane increases rapidly under the influence of pressure. When the pressure is greater than 10 MPa, the adsorption of pentane in the slit reaches near saturation, and the adsorption of pentane increases slowly with the increase of pressure. Under different pressure conditions, the change in pentane adsorption capacity with temperature is shown in Figure 3. When the pressure is low (5 MPa), the adsorption of pentane is greatly affected by temperature because the adsorption effect of the mineral wall under low pressure is the main factor affecting the adsorption capacity of *n*-pentane, and the adsorption effect is greatly affected by molecular thermal motion, so the adsorption of pentane under low pressure is greatly affected by temperature. However, with the increase of pressure (25 and 50 MPa), the role of pressure gradually becomes dominant. Under high pressure, *n*-pentane is compressed and its density increases, which leads to an increase in the interaction between gases. In contrast, the influence of adsorption becomes less obvious, so under high pressure, the adsorption of *n*-pentane is less affected by temperature. The variation of the local adsorption density of *n*-pentane with pressure at a temperature of 370 K is shown in Figure 4. As the pressure increases, the adsorption density of pentane in each adsorption layer gradually increases, and the

https://doi.org/10.1021/acsomega.4c06105
ACS Omega 2024, 9, 40145−40153

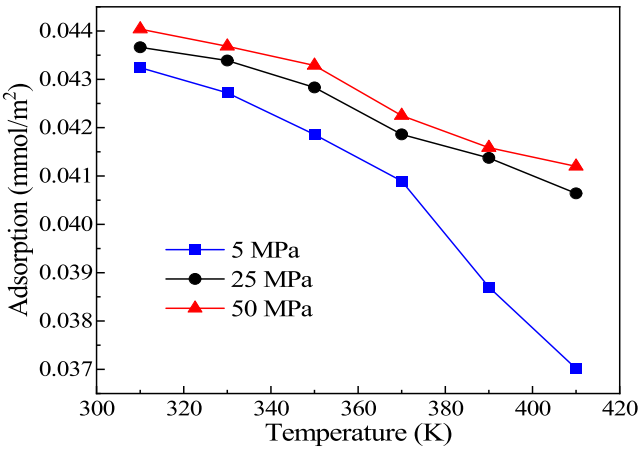

Figure 3. Curves of different adsorption capacities with temperature.

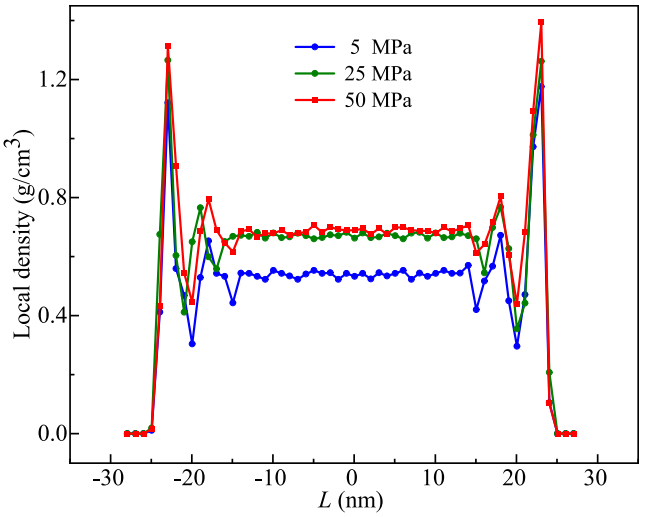

Figure 4. Local adsorption density of *n*-pentane varies with pressure.

increase is more significant at lower pressures. This further confirms that when the pressure reaches 25 MPa, the adsorption capacity of pentane in the slit reaches a nearly saturated state, and as the pressure increases, the adsorption capacity increases less.

$$\rho = \frac{N \times M_{\text{pentane}}}{N_A \times V} \quad (3)$$

here, N is the number of pentane adsorbed, M is the molar mass of pentane, g/mol, N_A is Avogadro's constant, and V is the pore volume of the slit, mL.

At 25 MPa, the adsorption capacity of pentane basically reaches a completely saturated state, and the adsorption capacity of pentane decreases linearly with the increase of temperature, indicating that under the same pressure conditions, high temperature is not conducive to the adsorption of *n*-pentane by minerals, mainly because the adsorption of *n*-pentane by silica slit is physical adsorption. When the temperature rises, the thermal movement of *n*-pentane molecules increases. With the increase of kinetic energy, the probability of escaping the binding force of the pore wall increases and the adsorption capacity of *n*-pentane decreases.

3.2. Changes in Pentane Adsorption with Aperture.

The pentane adsorption isotherms under different apertures are shown in Figure 5. Since the aperture has such a great

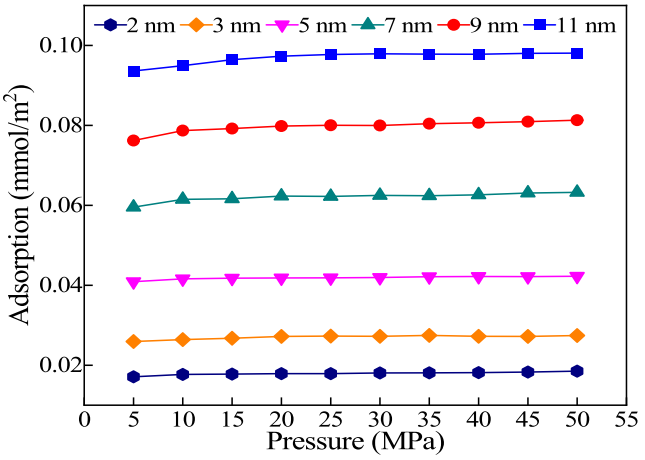

Figure 5. 370 K hydroxyl-modified isotherm adsorption line with different apertures.

influence on pentane adsorption, the effect of pressure becomes less obvious. At any pressure, the adsorption capacity of large pores is greater than that of small pores. The amount of adsorption. The calculated changes in pentane adsorption capacity with an aperture at a pressure of 25 MPa and a temperature of 370 K are shown in Figure 6. When the

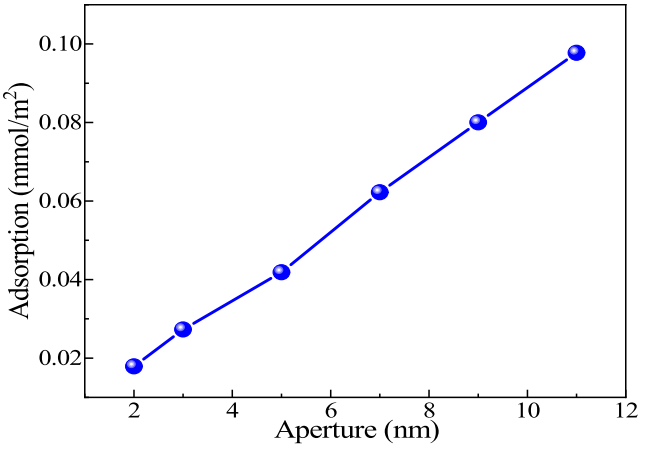

Figure 6. Adsorption capacity changes with aperture.

aperture is small, the number of pentane molecules that can enter the pores is limited, and the number of adsorption layers is limited by the limited space, so the adsorption capacity is small. With the increase of aperture, the adsorption capacity of pentane increases linearly because under a high pressure of 25 MPa, the adsorption capacity of pentane in the slit is basically in a saturated state, and the influence of other factors on pentane is not so obvious at this time. The larger the aperture, the larger the adsorption space of *n*-pentane, so the adsorption capacity increases linearly with the increase of aperture.

The adsorption configuration diagram of pentane in different pore size slits has been exported, as shown in Figure 7. The pentane molecules inside the blue boxes on both sides of the slits represent the part that exists on the surface of the formation in an adsorption state, located within 0.9 nm of the

https://doi.org/10.1021/acsomega.4c06105
ACS Omega 2024, 9, 40145−40153

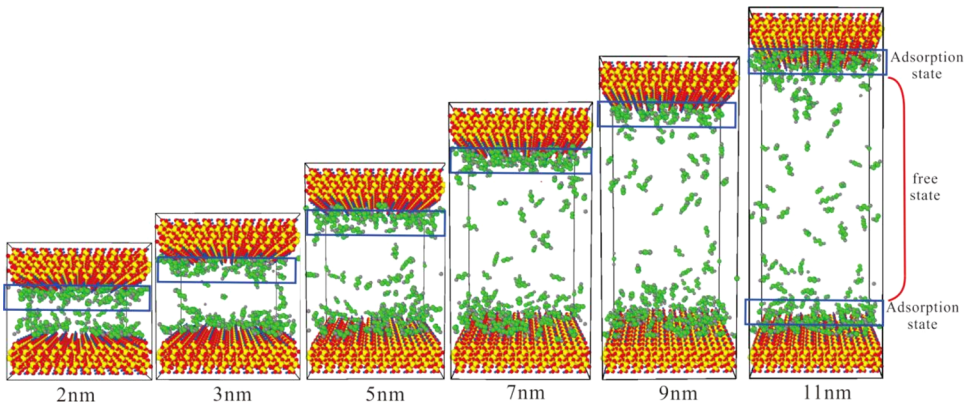

Figure 7. Adsorption configuration of pentane in narrows with different apertures.

near wall surface. The middle part represents molecules that exist in a free state in narrow spaces. Oil and gas molecules that exist in free form are more easily extracted, which we refer to as the easily accessible portion. On the contrary, oil and gas molecules that exist in an adsorbed state are difficult to mobilize. It is not difficult to see that as the pore size increases, there is little change in the adsorbed pentane molecules. The adsorbed molecules are attracted by the slit and exist. Therefore, under the same surface properties and external stable pressure conditions of the slit, the adsorbed molecules remain unchanged. As the pore size increases, the number of free pentane molecules gradually increases. The proportion of adsorbed pentane in different pore size slits is calculated as a function of pore size, as shown in Figure 8. When the pore size

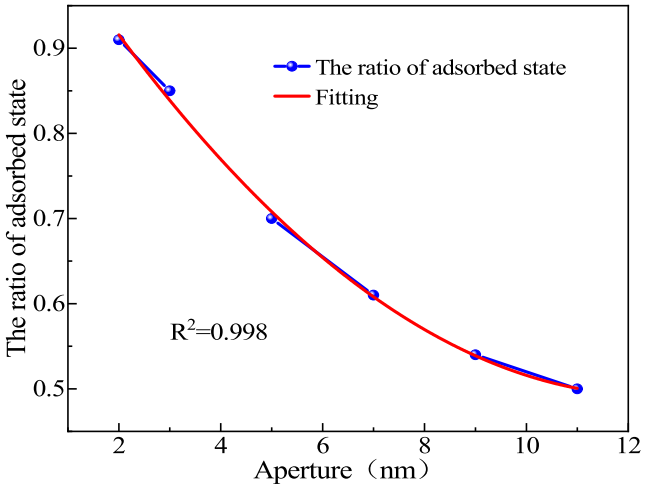

Figure 8. Changes in the proportion of adsorbed pentane with pore size.

is 2 nm, the proportion of adsorbed pentane molecules is as high as 90%. As the pore size increases, the proportion of adsorbed pentane molecules gradually decreases. When the pore size is greater than 11 nm, the proportion of adsorbed pentane molecules begins to be less than 50%. As the pore size increases, the proportion of adsorbed pentane molecules gradually decreases, the availability of oil and gas increases, and oil and gas are more easily extracted.

In order to further study the spatial distribution characteristics and quantity changes of *n*-pentane molecules in the silica slit, the density distribution curve of *n*-pentane molecules along the direction perpendicular to the pore wall is drawn. At 370 K and 25 MPa, the local density distribution of *n*-pentane molecules in the silica slit with different apertures is shown in Figure 9. It can be seen that under the same conditions, *n*-

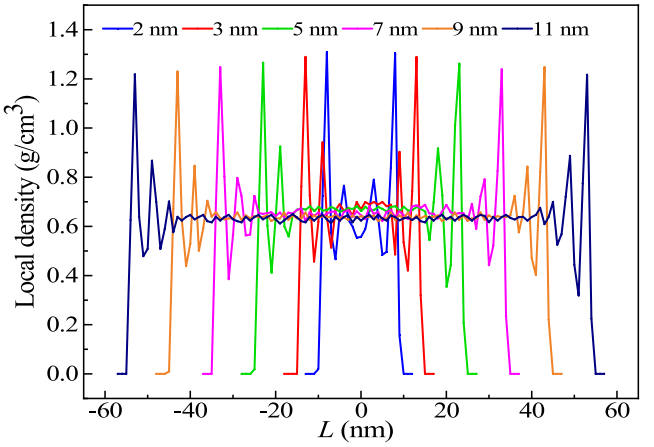

Figure 9. Local density distribution of different apertures.

pentane forms two adsorption layers in the slit with an aperture of 2 nm, the peak density is high, and most of *n*-pentane exists in the adsorption state. With the increase of aperture, the number of adsorbed layers increases and the density of the adsorbed phase decreases. In this case, *n*-pentane exists in both adsorbed and free states. The local density of the intermediate-free pentane decreases with the increase of aperture because in the small aperture, the force of the slit on the intermediate-free pentane is still significant, and the middle of the slit can still adsorb more pentane molecules, so the local density is larger.

This study used a joint atom model; *n*-pentane is uncharged in this model, and the van der Waals force acts as the main force between *n*-pentane and the slit, which has an important effect on the adsorption of *n*-pentane in the nanopore. In order to study the microscopic mechanism of the aperture affecting pentane adsorption, the relationship between the van der Waals force between the slit and alkane and the aperture is calculated, as shown in Figure 10. At this time, the van der Waals force between pentane and the slit is negative, showing mutual attraction. With the increase of aperture, the van der Waals force between pentane and the slit increases, which further shows that the adsorption capacity of alkanes increases with the increase of aperture.

https://doi.org/10.1021/acsomega.4c06105
ACS Omega 2024, 9, 40145−40153

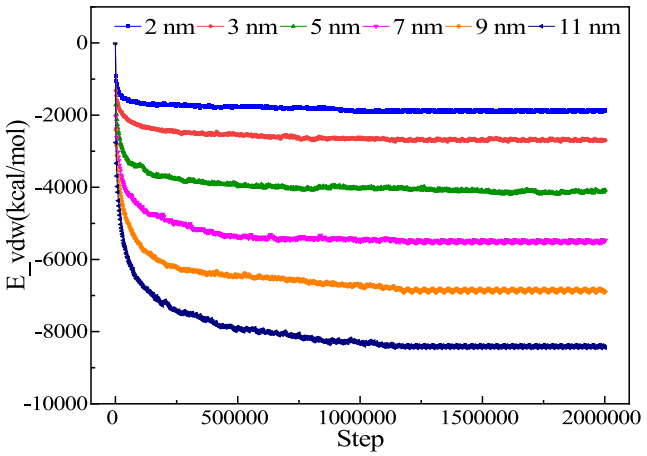

Figure 10. Van der Waals forces between pentane and the slit change with aperture.

3.3. Variation of Pentane Adsorption with Wettability. In order to characterize the quantitative relationship between wettability and pentane adsorption, the wettability of the mineral surface was quantified by the wetting contact angle, and the quantitative relationship between the wetting contact angle and pentane adsorption was obtained. The surfaces of 100, 50, and 25% hydroxyl-modified silica have water-wetting contact angles of 27.3, 37.9, and 46.8° respectively. The water-wetting contact angles of unmodified, methyl-modified, and $(CH_2)_4CH_3$-modified silica surfaces are 58.5, 84.9, and 105.1° respectively. The larger the wetting contact angle, the more lipophilic the surface.[42] The variation of adsorption isotherm with wettability at a 5 nm aperture and 370 K temperature is calculated, as shown in Figure 11. It can be found that in

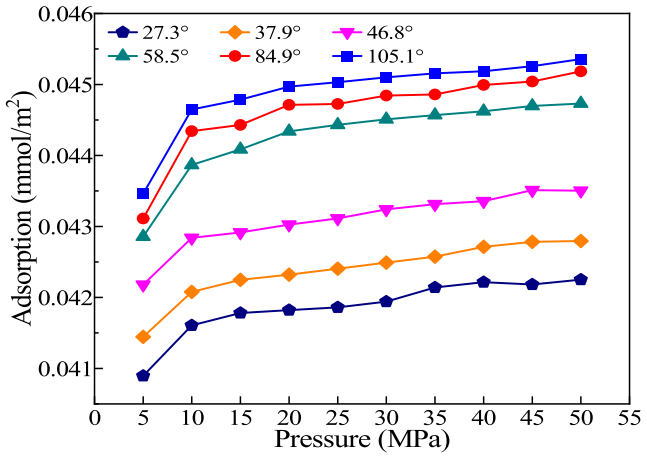

Figure 11. Adsorption isotherms with different wettabilities.

nanoslits with different wettabilities, the adsorption amount of pentane increases greatly with the increase of pressure before 10 MPa. After reaching 10 MPa, the adsorption capacity gradually becomes saturated, and the adsorption capacity gradually decreases due to the influence of pressure.

When the pressure is 25 MPa and the temperature is 370 K, the relationship between the adsorption capacity of pentane and the wetting contact angle is calculated, as shown in Figure 12, which can be divided into two sections: one is silica modified by hydrophilic groups, and the other is silica modified by lipophilic groups. Its distribution can be regarded as a

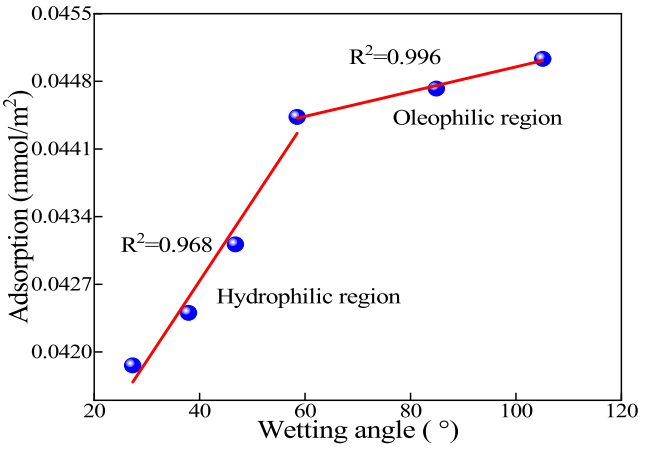

Figure 12. Variation of adsorption capacity with wetting angle.

piecewise function. The adsorption amount of pentane in the hydroxyl segment increases rapidly with the increase of wetting contact angle. The quantitative relationship between the adsorption amount and the wetting contact angle is fitted, as shown in Formula 4. Because hydroxyl is hydrophilic, the decrease of hydroxyl greatly increases the oil-repellent ability of the mineral surface. As a kind of oil component, the adsorption capacity of pentane is greatly influenced by hydroxyl, so the adsorption capacity of pentane is greatly influenced by the proportion of hydroxyl modification. For the non-hydroxyl segment, the adsorption amount of pentane increases with the increase of lipophilicity, but the range of the increase is small. The fitted quantitative relationship between the adsorption amount and the wetting contact angle is shown in Formula 5. Because there is an attraction between the hydrocarbon group and pentane, its attraction effect on pentane is not as obvious as that of the hydroxyl group on pentane. On the whole, the adsorption capacity of pentane increases with the increase of wetting contact angle.

$$Y = 0.039 + 8.25 \times 10^{-5} \times X \quad (4)$$

$$Y = 0.043 + 1.28 \times 10^{-5} \times X \quad (5)$$

In the formula, Y is the number of moles of pentane adsorbed per unit area, mmol/m^2, and X is the water-wetting contact angle of the silica surface,°.

The pentane adsorption configuration diagram is exported in a 5 nm slit with different wettabilities, as shown in Figure 13. Here, we can intuitively see that as the wetting contact angle increases, the wall hydrophilicity becomes stronger and more pentane molecules accumulate in the surface adsorption state, which to some extent reduces the efficiency of our oil and gas development. Therefore, in order to achieve efficient mining, we try to change the wettability of the wall surface as much as possible to make it hydrophilic. The calculated local density relationship of pentane adsorption in a slit with different wettabilities is shown in Figure 14. It can be seen that the number of pentane molecules in the first adsorption layer, the second adsorption layer, and the middle free state all increases with the increase of wetting contact angle. Because of the smaller pore size, as the lipophilicity of the mineral surface increases, the pentane in various parts of the slit is affected by surface attraction. The calculated van der Waals forces between surfaces with different wettabilities and pentane are shown in Figure 15. With the increase of wetting contact angle, the van

https://doi.org/10.1021/acsomega.4c06105
ACS Omega 2024, 9, 40145−40153

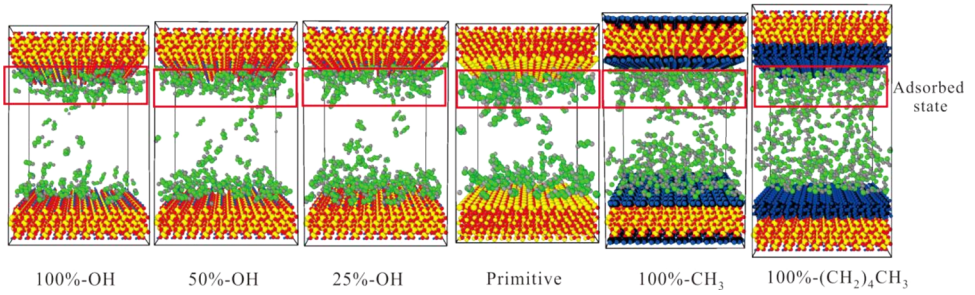

Figure 13. Adsorption configuration of pentane in slits with different wettabilities.

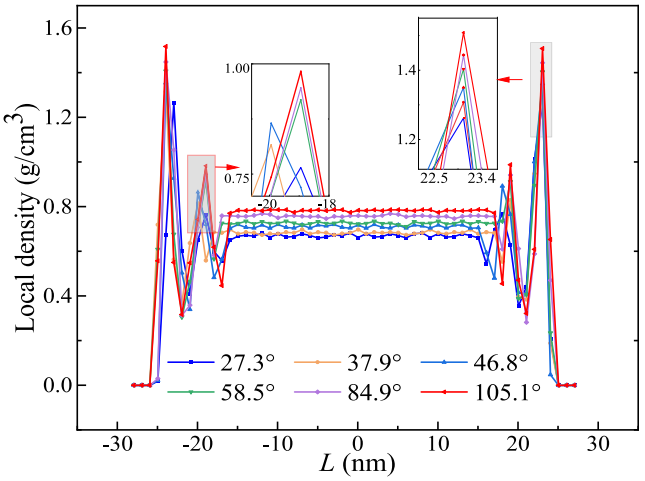

Figure 14. Variation of the local density of pentane adsorption with wetting angle.

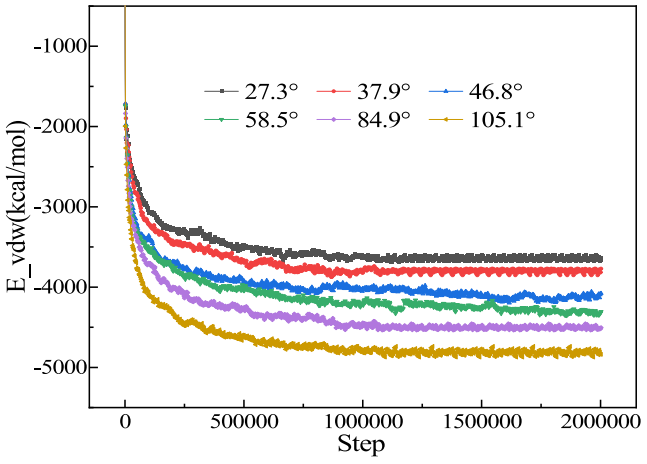

Figure 15. Van der Waals force between pentane and slit varies with wetting angle.

der Waals force between the slit and pentane increases, which indicates that the adsorption capacity of pentane on the mineral surface increases and further proves that the adsorption capacity of pentane increases with the increase of lipophilicity on the mineral surface.

4. CONCLUSIONS

In this study, the GCMC method was used to investigate the adsorption law of *n*-pentane in silica nanoparticles with various apertures and modified groups. The main conclusions of this research are as follows.

(1) The adsorption amount of pentane is greatly affected by temperature under low-pressure conditions and is less affected by temperature under high-pressure conditions. When the pressure is less than 10 MPa, pentane's adsorption amount increases obviously with the increase of pressure. When the pressure exceeds 10 MPa, pentane's adsorption amount increases slowly with the increase of pressure and finally reaches saturated adsorption at 25 MPa.

(2) Under high-pressure conditions, the adsorption amount of *n*-pentane increases linearly with the increased aperture of adsorption space. As the adsorbed pentane molecules gradually decrease, the availability of oil and gas increases, making it easier for oil and gas to be extracted.

(3) The van der Waals force between the mineral surface and pentane exhibits attraction. With the increase of wetting contact angle, the lipophilicity of the mineral surface increases, and the van der Waals force between the mineral and pentane also increases, resulting in an increase in the number of adsorbed states of pentane. The stronger the hydrophilicity of the wall, the fewer the pentane molecules adsorbed on the surface, which will improve the efficiency of our oil and gas extraction.

■ ASSOCIATED CONTENT

Data Availability Statement

The data that support the findings of this study are available within the article.

■ AUTHOR INFORMATION

Corresponding Author

Cao Yu − *Daqing Oilfield Exploration and Development Research Institute, Daqing 163000, China; State Key Laboratory of Continental Shale Oil, Daqing 163000, China;* orcid.org/0000-0002-1792-6673; Email: 1224538753@qq.com

Authors

Qinglong Xu − *Daqing Oilfield Exploration and Development Research Institute, Daqing 163000, China; State Key Laboratory of Continental Shale Oil, Daqing 163000, China*

Fancong Meng − *Daqing Oilfield Exploration and Development Research Institute, Daqing 163000, China*

Xuwei Liang − *Daqing Oilfield Exploration and Development Research Institute, Daqing 163000, China;* orcid.org/0000-0001-9037-9453

Yahui Li − *Daqing Oilfield Exploration and Development Research Institute, Daqing 163000, China*

https://doi.org/10.1021/acsomega.4c06105
ACS Omega 2024, 9, 40145−40153

Xin Kang − *Daqing Oilfield Exploration and Development Research Institute, Daqing 163000, China*
Hao Lu − *Daqing Oilfield Exploration and Development Research Institute, Daqing 163000, China*
Qiubo Wu − *Daqing Oilfield Exploration and Development Research Institute, Daqing 163000, China*
Sen Yang − *Daqing Oilfield Exploration and Development Research Institute, Daqing 163000, China*

Complete contact information is available at: https://pubs.acs.org/10.1021/acsomega.4c06105

Notes

The authors declare no competing financial interest.

REFERENCES

(1) Zeng, K.; Jiang, P.; Lun, Z.; et al. Molecular simulation of carbon dioxide and methane adsorption in shale organic nanopores. *Energy Fuels* **2019**, *33* (3), 1785−1796.
(2) Curtis, J. B. Fractured shale-gas systems. *AAPG Bull.* **2002**, *86* (11), 1921−1938.
(3) Wang, X.; Cheng, H.; Chai, P.; et al. Pore characterization of different clay minerals and its impact on methane adsorption capacity. *Energy Fuels* **2020**, *34* (10), 12204−12214.
(4) Wang, X.; Liu, P.; Meng, Q.; et al. Physical selectivity on isotopologues of gaseous alkanes by shale pore network: Evidence from dynamic adsorption process of natural gas. *J. Nat. Gas Sci. Eng.* **2022**, *97*, No. 104252.
(5) Li, J.; Lu, S.; Xie, L.; et al. Modeling of hydrocarbon adsorption on continental oil shale: A case study on n-alkane. *Fuel* **2017**, *206*, 603−613.
(6) Zhu, C.; Qin, X.; Li, Y.; et al. Adsorption and dissolution behaviors of CO2 and n-alkane mixtures in shale: effects of the alkane type, shale properties and temperature. *Fuel* **2019**, *253*, 1361−1370.
(7) Chen, G.; Lu, S.; Zhang, J.; et al. Keys to linking GCMC simulations and shale gas adsorption experiments. *Fuel* **2017**, *199*, 14−21.
(8) Zou, C.; Dong, D.; Wang, S.; et al. Geological characteristics and resource potential of shale gas in China. *Pet. Explor. Dev.* **2010**, *37* (6), 641−653.
(9) Wu, Z.; He, S.; Han, Y.; et al. Effect of organic matter type and maturity on organic matter pore formation of transitional facies shales: a case study on Upper Permian Longtan and Dalong Shales in middle Yangtze region. *J. Earth Sci.* **2020**, *31* (2), 368−384.
(10) Chen, G.; Lu, S.; et al. Investigation of pore size effects on adsorption behavior of shale gas. *Mar. Pet. Geol.* **2019**, *109*, 1−8.
(11) Liu, B.; Shi, J.; Shen, Y.; Zhang, J.; et al. A molecular dynamics simulation of methane adsorption in graphite slit-pores. *Chin. J. Comput. Phys.* **2013**, *30* (5), 692−699.
(12) Chen, L.; Huang, D.; Li, Z.; et al. Study on methane adsorption in graphite slit-pores by molecular dynamics simulation. *J. Therm. Sci. Technol.* **2016**, *15* (2), 92−96.
(13) Tian, S. C.; Wang, T. Y.; Li, G. S.; et al. Molecular simulation of methane adsorption behavior in different shale kerogen types. *Nat. Gas Ind.* **2017**, *37* (12), 18−25.
(14) Amirmoshiri, M.; Zhang, L.; Puerto, M. C.; et al. Role of wettability on the adsorption of an anionic surfactant on sandstone cores. *Langmuir* **2020**, *36* (36), 10725−10738.
(15) Zhu, Y. Q.; Su, H.; Jing, Y.; Guo, J.; Tang, J. Methane adsorption on the surface of a model of shale: a density functional theory study. *Appl. Surf. Sci.* **2016**, *387*, 379−384.
(16) Zhao, J.; Wang, Z.; Guo, P. Microscopic simulation of methane adsorption in organic matter. *Ind. Eng. Chem. Res.* **2019**, *58* (8), 3523−3530.
(17) Wu, B.; Liu, Y.; Lv, Y.; Zhang, J.; Xu, Y.; Hou, D. Modeling of multilayer water adsorption and condensation in slits of cement minerals by molecule simulation and adsorption isotherm. *Constr. Build. Mater.* **2024**, *421*, No. 135571.
(18) Lu, S. F.; Shen, B. J.; Xu, C.; et al. Study on adsorption behavior and mechanism of shale gas by using GCMC molecular simulation. *Earth Science* **2018**, *43* (5), 1783−1791.
(19) Chen, G.; Lu, S.; Zhang, J.; et al. Research of CO2 and N2 adsorption behavior in K-Illite slit pores by GCMC method. *Sci. Rep.* **2016**, *6* (1), No. 37579.
(20) Zhang, L.; Liu, C.; Li, Q. Molecular simulations of competitive adsorption behavior between CH4-C2H6 in K-Illite clay at super-critical conditions. *Fuel* **2020**, *260*, No. 116358.
(21) Collell, J.; Galliero, G.; Gouth, F.; et al. Molecular simulation and modelisation of methane/ethane mixtures adsorption onto a microporous molecular model of kerogen under typical reservoir conditions. *Microporous Mesoporous Mater.* **2014**, *197*, 194−203.
(22) Zhou, J.; Jin, Z.; Luo, K. Insights into recovery of multi-component shale gas by CO2 injection: a molecular perspective. *Fuel* **2020**, *267*, No. 117247.
(23) Onawole, A. T.; Nasser, M. S.; Hussein, I. A.; et al. Theoretical studies of methane adsorption on Silica Kaolinite interface for shale reservoir application. *Appl. Surf. Sci.* **2021**, *546*, No. 149164.
(24) Jang, Y.; Chung, E. Influence of alkanes on lithium adsorption and desorption of a H2TiO3 ion sieve adsorbent in synthetic shale gas-produced water. *Ind. Eng. Chem. Res.* **2019**, *58* (48), 21897−21903.
(25) Falk, K.; Pellenq, R.; Ulm, F. J.; et al. Effect of chain length and pore accessibility on alkane adsorption in kerogen. *Energy Fuels* **2015**, *29* (12), 7889−7896.
(26) Chen, G.; Lu, S.; Liu, K.; et al. Critical factors controlling shale gas adsorption mechanisms on different minerals investigated using GCMC simulations. *Mar. Pet. Geol.* **2019**, *100*, 31−42.
(27) Liu, Y.; Wilcox, J. Molecular simulation of CO2 adsorption in micro-and mesoporous carbons with surface heterogeneity. *Int. J. Coal Geol.* **2012**, *104*, 83−95.
(28) Wang, X.; Zhai, Z.; Jin, X.; et al. Molecular simulation of CO2/CH4 competitive adsorption in organic matter pores in shale under certain geological conditions. *Pet. Explor. Dev.* **2016**, *43* (5), 841−848.
(29) Zhang, T.; He, Y.; Yang, Y.; et al. Molecular simulation of shale gas adsorption in organic-matter nanopore. *J. Nat. Gas Geosci.* **2017**, *2* (5−6), 323−332.
(30) Jian, X.; Xiangjun, L.; Lixi, L. Molecular simulation on the adsorption behaviors of methane in montmorillonite slit pores. *Acta Pet. Sin.* **2016**, *37* (8), 1021.
(31) Chen, G.; Lu, S.; Zhang, J.; et al. Research of CO2 and N2 adsorption behavior in K-Illite slit pores by GCMC method. *Sci. Rep.* **2016**, *6* (1), No. 37579.
(32) Xiong, J.; Liu, X.; et al. Adsorption behavior of methane on kaolinite. *Ind. Eng. Chem. Res.* **2017**, *56* (21), 6229−6238, DOI: 10.1021/acs.iecr.7b00838.
(33) Wang, S.; Feng, Q.; Javadpour, F.et al. In *Multiscale Modeling of Shale Apparent Permeability: an Integrated Study of Molecular Dynamics and Pore Network Model*, SPE Annual Technical Conference and Exhibition; OnePetro, 2017.
(34) Ross, D. J. K.; Bustin, R. M. Characterizing the shale gas resource potential of Devonian-Mississippian strata in the Western Canada sedimentary basin: application of an integrated formation evaluation. *AAPG Bull.* **2008**, *92* (1), 87.
(35) Zhao, J.; Wang, Z.; Guo, P.; et al. Molecular level investigation of methane and carbon dioxide adsorption on SiO2 surface. *Comput. Mater. Sci.* **2019**, *168*, 213−220.
(36) Altundal, O. F.; Haslak, Z. P.; Keskin, S. Combined GCMC, MD, and DFT Approach for Unlocking the Performances of COFs for Methane Purification. *Ind. Eng. Chem. Res.* **2021**, *60* (35), 12999−13012.
(37) Yang, Z.; Yin, Z.; Xue, W.; et al. Construction of Buertai coal macromolecular model and GCMC simulation of methane adsorption in micropores. *ACS Omega* **2021**, *6* (17), 11173−11182.
(38) Zeng, K.; Lu, T.; Jiang, P.; et al. Methane adsorption capacity measurement in shale matrix nanopores at high pressure by low-field NMR and molecular simulation. *Chem. Eng. J.* **2022**, *430*, No. 133151.

(39) Zhang, D.; Tang, H.; Zhang, X.; et al. Molecular simulation of methane adsorption in nanoscale rough slits. *J. Nat. Gas Sci. Eng.* **2022**, *102*, No. 104608.
(40) Dai, X.; Tian, S.; He, Y.; et al. Methane/Carbon Dioxide Adsorption and Diffusion Performances at Different Mineral Compositions and Buried Depth Conditions. *Energy Fuels* **2021**, *35* (19), 15567−15578.
(41) Wang, Z.; Yu, C.; Zhao, J.; et al. Molecular dynamics simulation for quantitative characterization of wettability transition on silica surface. *J. Mater. Res. Technol.* **2022**, *19*, 4371−4380.
(42) Nath, S. K.; Escobedo, F. A.; de Pablo, J. J. On the simulation of vapor−liquid equilibria for alkanes. *J. Chem. Phys.* **1998**, *108* (23), 9905−9911.
(43) Darden, T.; York, D.; Pedersen, L. Particle mesh Ewald: An N·log (N) method for Ewald sums in large systems. *J. Chem. Phys.* **1993**, *98* (12), 10089−10092.

https://doi.org/10.1021/acsomega.4c06105
ACS Omega 2024, 9, 40145−40153